Original Article

Journal of Tissue Engineering
Volume 6: 1–17

DOI: 10.1177/2041731415609298
tej.sagepub.com
SAGE

Deletion of the nuclear localization sequence and C-terminus of parathyroid hormone–related protein decreases osteogenesis and chondrogenesis but increases adipogenesis and myogenesis in murine bone marrow stromal cells

Blake E Hildreth III[1], Krista M Hernon[2], Wessel P Dirksen[1], John Leong[1], Wachiraphan Supsavhad[1], Prosper N Boyaka[1], Thomas J Rosol[1] and Ramiro E Toribio[2]

Abstract

The N-terminus of parathyroid hormone–related protein regulates bone marrow stromal cell differentiation. We hypothesized that the nuclear localization sequence and C-terminus are involved. MicroRNA and gene expression analyses were performed on bone marrow stromal cells from mice lacking the nuclear localization sequence and C-terminus (*Pthrp*$^{\Delta/\Delta}$) and age-matched controls. Differentiation assays with microRNA, cytochemical/histologic/morphologic, protein, and gene expression analyses were performed. *Pthrp*$^{\Delta/\Delta}$ bone marrow stromal cells are anti-osteochondrogenic, pro-adipogenic, and pro-myogenic, expressing more *Klf4*, *Gsk-3*β, *Lif*, *Ct-1*, and microRNA-434 but less β-*catenin*, *Igf-1*, *Taz*, *Osm*, and microRNA-22 ($p \leqslant 0.024$). *Pthrp*$^{\Delta/\Delta}$ osteoblasts had less mineralization, osteocalcin, *Runx2*, *Osx*, *Igf-1*, and *leptin* ($p \leqslant 0.029$). *Pthrp*$^{\Delta/\Delta}$ produced more adipocytes, *Ppar*γ, and *aP2*, but less *Lpl* ($p \leqslant 0.042$). *Pthrp*$^{\Delta/\Delta}$ cartilage pellets were smaller with less *Sox9* and *Pth1r*, but greater *Col2a1* ($p \leqslant 0.024$). *Pthrp*$^{\Delta/\Delta}$ produced more myocytes, *Des*, and *Myog* ($p \leqslant 0.021$). MicroRNA changes supported these findings. In conclusion, the nuclear localization sequence and C-terminus are pro-osteochondrogenic, anti-adipogenic, and anti-myogenic.

Keywords

Parathyroid hormone–related protein, nuclear localization sequence, C-terminus, bone marrow stromal cell, differentiation

Received: 7 May 2015; accepted: 1 September 2015

Introduction

Parathyroid hormone–related protein (PTHrP) is a pleiotropic hormone that is widely expressed during embryonic development and post-natal life. PTHrP plays a vital role in many physiologic processes, including the regulation of skeletal morphogenesis and post-natal bone mass.[1,2] The main effects of PTHrP are attributed to its amino-terminus (N-terminus; amino acids 1–36), where it is equipotent with parathyroid hormone (PTH) at the common PTH/

[1]Department of Veterinary Biosciences, College of Veterinary Medicine, The Ohio State University, Columbus, OH, USA
[2]Department of Veterinary Clinical Sciences, College of Veterinary Medicine, The Ohio State University, Columbus, OH, USA

Corresponding author:
Ramiro E Toribio, Department of Veterinary Clinical Sciences, College of Veterinary Medicine, The Ohio State University, 601 Vernon L. Tharp Street, Columbus, OH 43210, USA.
Email: toribio.1@osu.edu

PTHrP receptor (PTH1R). While PTH functions primarily as an endocrine hormone in the bone and kidney, PTHrP is not normally present in circulation, acting primarily as a local regulator of cellular proliferation, differentiation, and survival.[3] In addition, unlike PTH, PTHrP has multiple additional functional domains, including a mid-region (amino acids 37–66), a nuclear localization sequence (NLS; 67–106), and a carboxy-terminus (C-terminus; 107–139).[3,4] Post-translational processing produces a family of peptides containing one or more of these regions, contributing to the protein's ability to function in an autocrine, paracrine, and intracrine manner.[3]

The role of skeletal-derived PTHrP was first observed in the PTHrP knockout mouse, which had abnormal endochondral ossification, increased and premature ossification, chondrodysplastic dwarfism, and neonatal lethality.[1] It was revealed that PTHrP is an endogenous skeletal anabolic agent and regulator of longitudinal bone growth by controlling growth plate chondrogenesis. The inability of PTH to complement or replace the skeletal role of PTHrP and the fact that overexpression of constitutively active PTH1R does not rescue all of the skeletal features of the PTHrP knockout mouse indicate that not all the functions of PTHrP are restricted to its N-terminal PTH-like domain.[5] To elucidate the functionality of additional domains of PTHrP in skeletal development, we created a mouse lacking the NLS and C-terminus, the *Pthrp*$^{\Delta/\Delta}$ mouse.[4] Similar to the PTHrP knockout mouse, the *Pthrp*$^{\Delta/\Delta}$ mouse is chondrodysplastic. However, unlike the PTHrP knockout mouse, which is characterized by abnormal endochondral ossification, increased and premature ossification, chondrodysplastic dwarfism, and neonatal lethality, the *Pthrp*$^{\Delta/\Delta}$ mouse has reduced skeletal mineralization, decreased osteochondrogenesis, and survives longer into the perinatal period. This indicates that the NLS and C-terminus are required for skeletogenesis and survival. This also emphasizes (1) the skeletal importance of the intracrine function of PTHrP facilitated by its NLS, whereby the protein is not secreted and exerts intracellular effects completely independent of binding to cell surface PTH1R and/or (2) the ability of secreted PTHrP to function in a PTH1R-independent manner, potentially through yet-to-be-characterized receptor systems for the NLS and/or C-terminus.

Bone marrow stromal cells (BMSCs) are capable of differentiating into multiple mesenchymal lineages, including osteoblasts, adipocytes, chondrocytes, and myocytes. However, the mechanisms regulating lineage specification are not fully understood. Haploinsufficiency for PTHrP in mice results in decreased bone mass, decreased and abnormal growth plate chondrogenesis, and increased bone marrow adipogenesis by 3 months of age.[6] This indicates that PTHrP influences BMSC differentiation in a pro-osteogenic, pro-chondrogenic, and anti-adipogenic manner. It has since been demonstrated that the N-terminus of exogenous PTH and PTHrP promotes osteogenesis and chondrogenesis at the cost of adipogenesis.[7,8] These effects contribute to the clinical bone-forming effects of N-terminal PTH and, to a lesser-investigated extent, PTHrP. On the other hand, the role of PTH and PTHrP in myogenic differentiation is unknown.

MicroRNAs (miRs) control gene and protein function by regulating existing messenger RNAs (mRNAs). Therefore, miRs can more rapidly affect gene and protein activity than traditional transcriptional regulation. Even though miRs regulate BMSC differentiation and their progeny, little information exists on the influence of PTHrP on miRs.[9–15]

Due to the fact that we have demonstrated (1) a decrease in the master transcriptional regulators of osteogenesis and chondrogenesis, Runx2 and Sox9, respectively, in the osteopenic and chondrodysplastic long bones of *Pthrp*$^{\Delta/\Delta}$ mice in vivo and (2) pro-osteogenic effects of both the NLS and C-terminus of PTHrP that are distinct from those elicited by the N-terminus in pre-osteoblasts in vitro; we proposed that the skeletal phenotype of *Pthrp*$^{\Delta/\Delta}$ mice may result, in part, by involvement of the NLS and C-terminus of PTHrP in regulating the multilineage differentiation of BMSCs.[4,16] Based on (1) the pro-osteochondrogenic and anti-adipogenic effects of the N-terminus of PTHrP and (2) the pro-osteochondrogenic effects of the NLS and C-terminus, the purpose of this study was to investigate the role of the NLS and C-terminus of PTHrP in the multilineage differentiation of BMSCs.[4,7,8,16] In addition, we defined the miR signatures in both unstimulated and differentiated BMSCs from *Pthrp*$^{\Delta/\Delta}$ and control mice. We hypothesized that BMSCs from *Pthrp*$^{\Delta/\Delta}$ mice would demonstrate decreased osteogenesis and chondrogenesis but enhanced adipogenesis and potentially increased myogenesis.

Materials and methods

Mice

Pthrp$^{\Delta/\Delta}$ mice created by our laboratory by replacing exon 4 of PTHrP with an exon 4 lacking the sequence encoding PTHrP 67–137 (the NLS and C-terminus) were used.[4] Deletion of the NLS and C-terminus (PTHrP (67–137)) was confirmed by reverse transcription (RT)-polymerase chain reaction (PCR) demonstrating PTHrP 1–66 (*Pthrp*$^{\Delta/\Delta}$) mRNA in whole bone, skin, liver, kidney, lung, and placental extracts. The reading frame of PTHrP 1–66 was confirmed by sequencing.[4] Heterozygous and wild-type littermates served as controls. We have found no phenotypic or functional differences between neonatal heterozygous and wild-type mice (Toribio et al.[4] and unpublished results). All applicable institutional guidelines for the care and use of animals were followed and all experimentation was approved by the Institutional Animal Care and Use Committee (IACUC 2009A0162).

Isolation and propagation of BMSCs

At 3–5 days of age, *Pthrp*$^{\Delta/\Delta}$ and control mice were euthanized in accordance with IACUC guidelines. Genomic DNA was isolated from tail tips and PCR genotyping performed using 5′-AGATCCACACAGCCGAAATCAGA-3′ (forward) and 5′-AGCCCTGCTGAACACAGTGAA CA-3′ (reverse) primers. Long bone marrow cavities were flushed with standard growth medium (α-Minimum Essential Medium (MEM) with Glutamax™, 20% fetal bovine serum (FBS), 60 U/mL penicillin, and 60 µg/mL streptomycin (Invitrogen, Grand Island, NY, USA)) into T-25 flasks (BD Biosciences, San Jose, CA, USA). The medium was changed 5 days later and every 3–5 days until the adherent monolayer of BMSCs reached confluence. Cells were passaged with 0.25% trypsin (Invitrogen) into T-75 flasks. The medium was changed every 3 days until the adherent monolayer was confluent and passaged again prior to use. Fourth passage BMSCs were used for all experimentation. Previous studies have demonstrated that mouse and human third to fourth passage BMSCs have comparable purity as those obtained by flow cytometry or negative selection techniques.[17–20]

Osteo-, adipo-, chondro-, and myogenic differentiation

Pthrp$^{\Delta/\Delta}$ and control BMSCs were plated at 400,000 cells/well in 12-well plates coated with 2.6 µg/cm^2 fibronectin (BD Biosciences). Confluent cohorts were treated for 24 days with 2 mL of either (1) osteogenic media—standard growth medium (defined above), 10 nM dexamethasone (Sigma–Aldrich, Inc., St. Louis, MO, USA), 250 µM ascorbic acid (Thermo Fisher Scientific, Inc., Waltham, MA, USA), and 10 mM β-glycerophosphate (MP Biomedicals, Inc., Solon, OH, USA); (2) adipogenic media—standard growth medium, 1 µM dexamethasone, 0.01 mg/mL insulin, 0.5 mM 3-isobutyl-1-methylxanthine, and 0.2 mM indomethacin (Sigma–Aldrich); (3) chondrogenic media (StemXVivo™; R & D Systems, Inc., Minneapolis, MN) with 100 U/mL penicillin, and 100 µg/mL streptomycin (Invitrogen); or (4) myogenic media—Dulbecco's Modified Eagle Medium (DMEM) with Glutamax™, 10% FBS, 1% glucose, 60 U/mL penicillin, and 60 µg/mL streptomycin (Invitrogen). Myogenic medium was supplemented with 5 µM of 5-azacytidine (Sigma–Aldrich) for 24 h once every 6 days. Culture medium was collected and frozen at −80°C every 3 days and fresh differentiation medium applied.

Cytochemical assessment of osteogenesis

Osteogenesis was assessed by von Kossa staining and quantifying the area of mineralization. After 24 days, four to five replicates from each genotype were fixed with 95% ethanol for 15 min. The wells were then treated sequentially with 5% silver nitrate (Sigma–Aldrich) for 20 min in the dark and 0.5% hydroquinone (Acros Organics, Geel, Belgium) for 5 min under ultraviolet light, rinsing with sterile water before and after each step. The wells were then treated with 5% sodium thiosulfate (Thermo Fisher Scientific). Stained wells were imaged with a 12.5-megapixel resolution 16-bit digital camera (Model D2X; Nikon Instruments Inc., Melville, NY, USA). The area of mineralization (mm^2) was calculated from the automated tracings of the von Kossa–stained regions in the central 80% of each well (Image-Pro Plus v9.1; Media Cybernetics, Inc., Rockville, MD, USA).

Cytochemical assessment of adipogenesis

Adipogenesis was assessed by Oil Red O staining of adipocytes. After 24 days, four replicates from each genotype were fixed for 30 min with a 3.7% formaldehyde in phosphate-buffered saline (PBS) solution, pH = 7.4. The wells were then stained for 20 min with 1.3 mg/mL Oil Red O (Sigma–Aldrich) in 55% 2-propanol, rinsing with sterile water before and after each step. Adipocyte counts at 200× magnification in five random fields/well were averaged for an adipocyte count/high-powered field (hpf) for each well (Image-Pro Plus).

Morphometric, histologic, and immunohistochemical analyses of chondrogenesis

Chondrogenesis was assessed by the following:

1. Morphometric assessment of chondrogenesis—a cartilage pellet culture system was employed using BMSCs and the commercially available chondrogenesis differentiation media described above (StemXVivo™ R & D Systems), adhering to the manufacturer's instructions. The exact components present in this chondrogenesis differentiation media are proprietary (personal communication with the manufacturer's technical support). *Pthrp*$^{\Delta/\Delta}$ and control BMSCs were seeded in quadruplicate at 250,000 cells/well in 15-mL conical tubes containing 500 µL of chondrogenic medium. Cells were pelleted at 500 rcf for 5 min and treated with chondrogenic medium for 24 days, changing the media every 3 days. Cartilage pellets were then imaged at 90° using a digital camera (Nikon) and volumes calculated from the average radius calculated from orthogonal views (Image-Pro Plus).
2. Histologic and immunohistochemical (IHC) evaluation of chondrogenesis—four cartilage pellets for each genotype were formalin-fixed, embedded in paraffin, sectioned, and stained with (1) hematoxylin and eosin (H & E), (2) alcian blue (for

glycosaminoglycans), and (3) a commercially available type II collagen staining kit (Chondrex, Inc., Redmond, WA, USA) (to demonstrate type II collagen). Alcian blue staining was performed by treating the slides with a 1% alcian blue in 3% acetic acid solution, pH = 2.5, for 30 min. Slides were then rinsed with water and counterstained briefly with eosin. Type II collagen staining was performed as recommended by the manufacturer except for with the primary antibody we used (1) an overnight incubation and (2) a 1:50 antibody dilution based on our preliminary antibody optimization. Type II collagen IHC slides were then briefly counterstained with hematoxylin. Negative controls processed in parallel consisted of (1) cartilage pellets stained only with hematoxylin and (2) neonatal age-matched mouse skeletal muscle stained with both hematoxylin and anti-type II collagen antibody. The articular surfaces of neonatal age-matched mouse vertebral endplates served as positive controls for type II collagen IHC. Histologic descriptions for both *Pthrp*$^{\Delta/\Delta}$ and control cartilage pellets were generated.

Cytochemical and flow cytometric analyses of myogenesis

Myogenesis was assessed by the following:

1. Cytochemical analysis of myogenesis—myogenesis was confirmed by cytochemical staining for the muscle-specific protein desmin. *Pthrp*$^{\Delta/\Delta}$ and control BMSCs were plated in quadruplicate at 400,000 cells/well in two-well fibronectin-coated chamber slides (Nunc™ Lab-Tek™ Chamber Slide System; Thermo Fisher Scientific). After 24 days of myogenesis, cells were formalin-fixed and stained with a 1:100 dilution of a polyclonal goat anti-human/mouse desmin biotinylated antibody (R&D Systems). Desmin-positive myocytes were quantified at 400× magnification. Eight random fields per well were averaged within each well to give a myocyte count per hpf for each well (Image-Pro Plus). Antibody specificity was verified by a positive Western blot and IHC on mouse skeletal muscle and a negative Western blot and IHC on mouse calvarial MC3T3-E1 pre-osteoblasts (data not shown).
2. Intracellular anti-desmin flow cytometry—cells in four wells from each genotype from the 12-well plates were lifted with 0.25% trypsin (Invitrogen) at baseline and after 24 days of myogenic differentiation. Cells were (1) fixed and permeabilized using the Cytofix/Cytoperm Kit (BD Biosciences) and (2) labeled intracellularly with a 1:150 dilution of anti-desmin antibody and a 1:800 dilution of streptavidin–allophycocyanin. Desmin-positive cells were quantified at 40,000 events/s (Accuri™ C6 Flow Cytometer; BD Biosciences). At baseline, the percentage of cells that were desmin-positive was measured. After 24 days of myogenic differentiation, the fold change in the number of desmin-positive cells when compared to baseline and the overall number of desmin-positive cells were calculated.

Gene expression analyses by quantitative real-time PCR

Total RNA was extracted with TRIzol (Invitrogen) and purified using the RNeasy® Mini Kit's RNA cleanup protocol (Qiagen, Germantown, MD, USA). Complementary DNA (cDNA) was made using Superscript II reverse transcriptase (Invitrogen). Quantitative real-time PCR was performed by (1) denaturing at 94°C for 15 min and (2) denaturing, annealing, and elongation for 60 cycles of 94°C for 15 s, 57°C for 20 s, and 72°C for 10 s using SYBR Green mastermix (Qiagen) and the Lightcycler 480 Real-Time PCR system (Roche, Indianapolis, IN, USA). The three most stably expressed genes out of *Ppia*, *Ubc*, *β-actin*, and *Hprt* between genotypes at baseline and for each specific differentiation assay were used for normalization by geometric averaging. *Ppia*, *Ubc*, and *β-actin* were used at baseline and for osteogenic, adipogenic, and myogenic differentiation. *Ppia*, *Ubc*, and *Hprt* were used for chondrogenic differentiation. Symbols and primers for all genes are defined in Table 1. The mouse primer pairs used in this study were chosen from two to four different primer pairs designed for each particular gene. All primer pairs were designed using Primer-BLAST software (http://www.ncbi.nlm.nih.gov/tools/primer-blast). Primers were compared side-by-side using historical control mouse bone, fat, cartilage, or muscle tissue and the primer pair for each gene that had the best amplification and real-time PCR product melting characteristics was chosen. In order to confirm primer specificity, Real-time PCR products were verified by electrophoresis on a 2% agarose gel and ethidium bromide staining to confirm (1) a single amplification product and (2) an amplification product of the expected size. Real-time PCR product melting characteristics for each primer pair were similar between experimental *Pthrp*$^{\Delta/\Delta}$ and control samples and historical control tissues (mouse bone, fat, cartilage, or muscle) (Table 1):

1. Assessment of BMSC lineage commitment genes at baseline—*Pthrp*$^{\Delta/\Delta}$ and control BMSCs were plated in sextuplet in standard growth media at 400,000 cells/well in 12-well plates coated with 2.6 μg/cm^2 fibronectin (Sigma–Aldrich). At confluence, the following lineage commitment regulatory genes were analyzed: *Pthrp*, *Pth1r*, *Klf4*, *Zfp521*,

Table 1. Mouse-specific primers for real-time PCR quantification of gene expression.

Gene name (symbol)	Primer sequences	Predicted product size (bp), same as control tissue	Control tissue Tm (°C)	*Pthrp*$^{\Delta/\Delta}$ and control PCR product Tm (mean ± SD, (range))
Kruppel-like factor 4 (*Klf4*)	Fwd: 5′-GGAGAAGACACTGCGTCCAG-3′ Rev: 5′-GGGAAGTCGCTTCATGTGAGA-3′	76	82.2	82.0 ± 0.1 (81.9–82.1)
Glycogen synthase kinase-3 beta (*Gsk-3β*)	Fwd: 5′-CAGGCTGTGTGTTGGCTGAATTGT-3′ Rev: 5′-AGACCTTTGTCCAAGGATGTGCCT-3′	186	79.4	79.2 ± 0.1 (79.0–79.4)
Beta-catenin (β-*catenin*)	Fwd: 5′-GCCATTGTACGCACCATGCAGAAT-3′ Rev: 5′-AGTGTCGTGATGGCGTAGAACAGT-3′	188	84.0	83.9 ± 0.1 (83.8–84.0)
Tafazzin (*Taz*)	Fwd: 5′-CAGACATCTGCTTCACCAAGGA-3′ Rev: 5′-TTGAAGCGCAGGAACTCAGAACT-3′	190	81.9	81.9 ± 0.1 (81.8–82.1)
Insulin-like growth factor-1 (*Igf-1*)	Fwd: 5′-GACCGAGGGGCTTTTACTTC-3′ Rev: 5′-CAACACTCATCCACAATGCC-3′	88	82.3	81.9 ± 0.1 (81.8–82.1)
Oncostatin M (*Osm*)	Fwd: 5′-GAGTACCAGGACCCAGTATGC-3′ Rev: 5′-TCAGGATGAGGAGACTGAGGG-3′	75	79.4	79.4 ± 0.1 (79.2–79.6)
Zinc finger protein 521 (*Zfp521*)	Fwd: 5′-GACGCCAACAGCACACAGTTGAAA-3′ Rev: 5′-GCTGCAGAGTTTGCACTCATGGTT-3′	195	82.1	82.0 ± 0.1 (81.9–82.2)
Parathyroid hormone-related protein (*Pthrp*)	Fwd: 5′-AGTGTCCTGGTATTCCTGCTC-3′ Rev: 5′-ATGCAGTAGCTGATGTTCAGACAC-3′	108	86.5	86.4 ± 0.1 (86.1–86.6)
PTH 1 receptor (*Pth1r*)	Fwd: 5′-CGCTGGTGACGTCAGACGATGTC-3′ Rev: 5′-CGGGGTAGAACTTTCCCGGTGC-3′	198	84.3	84.0 ± 0.1 (83.8–84.2)
Low-density lipoprotein receptor-related protein 6 (*Lrp6*)	Fwd: 5′-TTGATGGTGCCCTTCGATGCAATG-3′ Rev: 5′-TGCTGGCTCCTCAGTTGGATAACA-3′	200	82.6	82.5 ± 0.2 (82.4–82.8)
Leukemia inhibitory factor (*Lif*)	Fwd: 5′-CGCCAATGCTCTCTTCATTTCC-3′ Rev: 5′-TAGGCGCACATAGCTTTTCCA-3′	80	79.5	79.4 ± 0.1 (79.3–79.6)
Cardiotrophin 1 (*Ct-1*)	Fwd: 5′-GAGCCAGAGGGAGGGAAGTC-3′ Rev: 5′-CTCCCTGTTGCTGCACGTATT-3′	158	82.9	82.7 ± 0.1 (82.6–82.9)
Protein kinase A (*Pka*)	Fwd: 5′-GATGTTCTCCCACCTACGGC-3′ Rev: 5′-AAAGGTCAGGACGATCTGCG-3′	82	84.1	83.8 ± 0.02 (83.8–83.9)
Protein kinase C (*Pkc*)	Fwd: 5′-ACCACCATTCAAGCCCAAAGT-3′ Rev: 5′-CAAACTGGGGGTTGACATACGA-3′	158	80.8	80.9 ± 0.01 (80.8–80.9)
Runt-related transcription factor 2 (*Runx2*)	Fwd: 5′-CCTCTTCAGCGCAGTGACACCG-3′ Rev: 5′-ACGTCGCTCATCTTGCCGGG-3′	111	87.0	86.5 ± 0.1 (86.4–86.8)
Osterix (*Osx*)	Fwd: 5′-CTGCCTGACTCCTTGGGACC-3′ Rev: 5′-GGGGACTGGAGCCATAGTGA-3′	86	83.3	83.1 ± 0.1 (82.9–83.4)
Leptin (*Leptin*)	Fwd: 5′-TGACACCAAAACCCTCATCA-3′ Rev: 5′-TGAAGCCCAGGAATGAAGTC-3′	114	81.7	81.5 ± 0.1 (81.4–81.8)
Type I collagen, alpha 2 (*Col1a2*)	Fwd: 5′-TGGCAAGCCCGGAGAAAGGG-3′ Rev: 5′-GCTCCACTGGGACCTCGGCT-3′	141	84.8	84.6 ± 0.1 (84.5–84.8)

(Continued)

Table 1. (Continued)

Gene name (symbol)	Primer sequences	Predicted product size (bp), same as control tissue	Control tissue Tm (°C)	*Pthrp*$^{\Delta/\Delta}$ and control PCR product Tm (mean ± SD, (range))
EPH receptor B4 (*EphB4*)	Fwd: 5′-GAGGTCATGTCTTTTGGGGA-3′ Rev: 5′-CCGGTAGTCCTGTTCAATGG-3′	81	80.0	79.6 ± 0.1 (79.4–79.8)
Peroxisome proliferator-activated receptor gamma (*Pparγ*)	Fwd: 5′-TGCACTGCCTATGAGCACTTCACA-3′ Rev: 5′-AGTGTGGAGCAGAAATGCTGGAGA-3′	176	82.3	81.9 ± 0.03 (81.8–81.9)
CCAAT-enhancer-binding protein alpha (*C/ebpα*)	Fwd: 5′-ATAGACATCAGCGCCTACATCGAC-3′ Rev: 5′-TCCCGGGTAGTCAAAGTCACCG-3′	141	89.1	89.1 ± 0.2 (88.7–89.2)
CCAAT-enhancer-binding protein beta (*C/ebpβ*)	Fwd: 5′-GTTTCGGGACTTGATGCAAT-3′ Rev: 5′-GCCCGGCTAGACAGTTACAC-3′	91	83.6	83.4 ± 0.1 (83.2–83.5)
Adipsin (*Adipsin*)	Fwd: 5′-TCCGTGTACTTCGTGGCTCT-3′ Rev: 5′-CACGGAAGCCATGTAGGG-3′	120	87.3	86.9 ± 0.1 (86.7–86.9)
Adipocyte Protein 2 (*aP2*)	Fwd: 5′-GATGGTGACAAGCTGGTGGT-3′ Rev: 5′-TCCGACTGACTATTGTAGTGTTTGA-3′	129	79.9	79.8 ± 0.1 (79.7–79.8)
Lipoprotein lipase (*Lpl*)	Fwd: 5′-CTCGCTCTCAGATGCCCTAC-3′ Rev: 5′-CCACTGTGCCGTACAGAGAA-3′	117	80.0	79.9 ± 0.04 (79.8–79.9)
Sex determining region Y-box 9 (*Sox9*)	Fwd: 5′-AAGACTCTGGGCAAGCTCTGGA-3′ Rev: 5′-TTGTCCGTTCTTCACCGACTTCCT-3′	150	86.1	85.5 ± 0.04 (85.4–85.5)
Aggrecan (*Agg*)	Fwd: 5′-TTGCAGACCAGGAGCAATGT-3′ Rev: 5′-TCAGACCGATCCACTGGTAGT-3′	198	84.5	84.5 ± 0.06 (84.4–84.6)
Type II collagen, alpha 1 (*Col2a1*)	Fwd: 5′-ACCAGATTGAGAGCATCCGC-3′ Rev: 5′-CAGCCCTGGTTGGGATCAAT-3′	127	85.2	85.1 ± 0.02 (85.1–85.2)
Myogenin (myogenic factor 4) (*Myog*)	Fwd: 5′-CAATGCACTGGAGTTCGGT-3′ Rev: 5′-CACGATGGACGTAAGGGAGT-3′	94	83.0	82.6 ± 0.2 (82.4–82.9)
Desmin (*Des*)	Fwd: 5′-GTGAAGATGGCCTTGGATGT-3′ Rev: 5′-GCTGGTTTCTCGGAAGTTGA-3′	117	82.6	82.1 ± 0.1 (81.9–82.2)
Peptidylprolyl isomerase A (*Ppia*)	Fwd: 5′-CGCGTCTCCTTCGAGCTGTTTG-3′ Rev: 5′-TGTAAAGTCACCACCCTGGCACAT-3′	150	80.2	80.2 ± 0.2 (79.8–80.4)
Ubiquitin (*Ubc*)	Fwd: 5′-CGTCGAGCCCAGTGTTACCACCAAGAAGG-3′ Rev: 5′-CCCCCATCACACCCAAGAACAAGCACAAG-3′	112	80.1	80.0 ± 0.2 (79.6–80.3)
Beta-actin (β-*actin*)	Fwd: 5′-ATGAGCTGCCTGACGGCCAGGTCATC-3′ Rev: 5′-TGGTACCACCAGACAGCACTGTGTTG-3′	192	82.8	82.5 ± 0.2 (82.0–82.9)
Hypoxanthine-guanine phosphoribosyl-transferase (*Hprt*)	Fwd: 5′-GCTGGTGAAAAGGACCTCT-3′ Rev: 5′-CACAGGACTAGAACACCTGC-3′	249	79.9	79.7 ± 0.1 (79.5–79.9)

PCR: polymerase chain reaction; SD: standard deviation.
Gene names, gene symbols, and sequences for both the forward and reverse primers are listed. The predicted product size for each specific primer pair was verified by gel electrophoresis. Historical control PCR products were the same size as predicted for the specific primer pair. The PCR product melting temperatures for our experimental *Pthrp*$^{\Delta/\Delta}$ and control samples were similar to the historical control PCR products for each specific primer pair.

Lrp6, *Gsk-3β*, *β-catenin*, *Igf-1*, *Taz*, *Osm*, *Lif*, *Ct-1*, *Pka*, and *Pkc*.

2. Evaluation of lineage-specific genes after differentiation—after 24 days of growth in monolayer under distinct differentiation conditions in 12-well plates, the expression of the following genes was measured in –four to six replicates for both genotypes:
   (a) Osteogenesis: *Runx2, Osx, EphB4, Igf-1, Leptin, Col1a2, Pthrp, Pth1r;*
   (b) Chondrogenesis: *Sox9, Agg, Col2a1, Pthrp, Pth1r;*
   (c) Adipogenesis: *Ppary, C/ebpa, C/ebpβ, Adipsin, aP2, Lpl, Pthrp, Pth1r;*
   (d) Myogenesis: *Des, Myog, Pthrp, Pth1r*.

miR sequencing

miRs were sequenced for both genotypes at baseline (confluence) and after cells underwent differentiation. This was done to determine differentially regulated miRs that may influence lineage commitment, differentiation, and function. Total RNA from three to four biological replicates within each genotype were pooled, contributing equally to a total of 5 μg of total RNA. One of these pooled total RNA preparations was prepared for each genotype ($Pthrp^{\Delta/\Delta}$ and control) for each of the osteo-, chondro-, adipo-, and myogenesis assays. Two independent pooled total RNA preparations were prepared as described above for each genotype from different cohorts of $Pthrp^{\Delta/\Delta}$ and control mice at baseline (confluence) prior to differentiation, which allowed for direct statistical comparison (n = 2 total RNA preparations sequenced for each genotype at baseline). MiR libraries were generated using the NEBNext® Small RNA Library Prep Set for SOLiD (New England Biolabs, Ipswich, MA). Templated sequencing beads were produced via emulsion PCR with the EZ Bead system and sequenced with the SOLiD™ 5500 system (Applied Biosystems, Grand Island, NY, USA). In each sample, the total number of reads for each miR was normalized to the total number of reads for all the miRs and expressed as a number per million reads. MiRs with less than 500 reads were excluded. In the differentiation assays, the number of reads for each miR in $Pthrp^{\Delta/\Delta}$ samples was divided by the number of reads for that particular miR in controls and expressed as a fold change. Since a cut-off for what is a biologically relevant fold change in miRs has not been established, we arbitrarily selected and only reported fold changes exceeding 2.5-fold for the differentiation assays.

Osteocalcin assay

Osteocalcin (OCN) concentrations were measured in six wells at days 12 and 24 in the osteogenesis assays (Mouse Osteocalcin EIA kit; Biomedical Technologies Inc., Stoughton, MA, USA) according to the manufacturer's instructions. The OCN concentration for each well was normalized to the total amount of protein present in the same collected culture media sample.

Statistical analyses

The values are represented as mean ± 1 standard deviation. Lineage-specific cytochemical, morphometric, and flow cytometric indices, protein secretion, and real-time PCR ΔCT values were compared between genotypes with an unpaired t-test if normally distributed and of equal variance. Normally distributed data with unequal variances were compared with an unpaired t-test with Welch's correction. Non-normally distributed data were compared with a Mann–Whitney rank sum test. Baseline miR data were compared with an unpaired t-test. Analyses were performed with significance defined at $p < 0.05$ (Prism v6.00; GraphPad Software, Inc., San Diego, CA, USA). Assessment at baseline and individual multilineage differentiation assays were performed two independent times using separate cohorts of $Pthrp^{\Delta/\Delta}$ and control mice to ensure the reproducibility of the differentiation phenotypes reported.

Results

$Pthrp^{\Delta/\Delta}$ BMSCs have changes in gene and miR expression that indicate an anti-osteogenic, anti-chondrogenic, pro-adipogenic, and pro-myogenic phenotype

$Pthrp^{\Delta/\Delta}$ BMSCs expressed a significantly greater amount of *Klf4, Pth1r, Zfp521*, and *Lrp6* ($p \leq 0.002$) as determined by real-time PCR; however, the expression of *Gsk-3β* was increased with a concurrent decrease in *β-catenin* ($p \leq 0.024$) (Table 2). $Pthrp^{\Delta/\Delta}$ BMSCs expressed significantly less *Igf-1, Taz*, and *Osm* and increased *Lif, Ct-1*, and *Pkc* ($p \leq 0.026$). No differences were observed between genotypes for *Pka* and *Pthrp* (Table 2).

$Pthrp^{\Delta/\Delta}$ BMSCs at baseline expressed significantly less miR-22 ($p = 0.008$) and greater miR-434 ($p = 0.016$) when compared to control BMSCs (Table 3). The effects of these miR differences in $Pthrp^{\Delta/\Delta}$ BMSCs based on their known functions are decreased osteochondrogenesis and increased adipogenesis.[21,22]

Osteoblasts derived from $Pthrp^{\Delta/\Delta}$ BMSCs have decreased osteoblast maturation, function, and bone formation

$Pthrp^{\Delta/\Delta}$ BMSC-derived osteoblasts secreted significantly less OCN ($p \leq 0.029$) and produced a significantly smaller area of mineralization at day 24 ($p = 0.0004$) when compared to osteoblasts differentiated from control BMSCs (Figure 1). The expressions of *Runx2*, *Osx*, *Igf-1*, and *leptin* were significantly decreased in $Pthrp^{\Delta/\Delta}$ osteoblasts ($p \leq 0.018$). No differences in expression between

Table 2. Expression of lineage commitment regulatory genes.

Gene	$Pthrp^{\Delta/\Delta}$	Control	*p*-Value
Klf4	2.03 ± 0.11	1.01 ± 0.15	<0.0001
Zfp521	3.36 ± 0.32	1.01 ± 0.16	<0.0001
Lrp6	1.46 ± 0.09	1.00 ± 0.09	<0.0001
Gsk-3β	1.26 ± 0.14	1.01 ± 0.18	0.024
β-catenin	0.64 ± 0.04	1.01 ± 0.19	0.001
Igf-1	0.33 ± 0.004	1.02 ± 0.21	<0.0001
Taz	0.73 ± 0.04	1.01 ± 0.18	0.005
Osm	0.36 ± 0.02	1.01 ± 0.16	<0.0001
Lif	1.19 ± 0.08	1.00 ± 0.08	0.002
Ct-1	1.70 ± 0.26	1.01 ± 0.17	0.0003
Pka	1.09 ± 0.11	1.01 ± 0.11	NS
Pkc	1.62 ± 0.33	1.01 ± 0.16	0.026
Pthrp	1.65 ± 0.44	1.08 ± 0.45	NS
Pth1r	2.18 ± 0.18	1.02 ± 0.21	0.002

NS: not statistically significant; BMSC: bone marrow stromal cell; SD: standard deviation.
$Pthrp^{\Delta/\Delta}$ BMSCs possess an anti-osteogenic, anti-chondrogenic, pro-adipogenic, and pro-myogenic gene signature. Gene symbols are defined in Table 1. Values represent mean ± SD of six replicates. Findings are representative of two independent experiments.

Table 3. Expression of lineage commitment regulatory miRs.

miR	$Pthrp^{\Delta/\Delta}$ reads	Control reads	*p*-Value
miR-22	346,590 ± 8308	430,080 ± 6801	0.008
miR-30d	15,191 ± 740	13,208 ± 77	0.064
miR-193b	833 ± 21	1061 ± 95	0.081
miR-199b	115,514 ± 3629	80,949 ± 13,989	0.077
miR-221	18,531 ± 2302	27,229 ± 2221	0.062
miR-434	3060 ± 102	2208 ± 117	0.016

miR: microRNA; BMSC: bone marrow stromal cell; SD: standard deviation.
Similar to the gene expression analysis, $Pthrp^{\Delta/\Delta}$ BMSCs possess an anti-osteogenic, anti-chondrogenic, pro-adipogenic, and pro-myogenic miR signature. Values represent mean ± SD of two replicates.

genotypes were observed for *Col1a2*, *EphB4*, *Pthrp*, and *Pth1r* (Figure 1).

miR sequencing at day 24 revealed that $Pthrp^{\Delta/\Delta}$ osteoblasts expressed a greater amount of miR-204 (+6.6-fold), 450a (+4.0-fold), 410 (+3.6 fold), 16-2 (+3.0-fold), 18a (+2.8-fold), 146b (+2.7-fold), 31 (+2.6-fold), and 19a (+2.5-fold) but a lesser amount of miR-223 (−2.5-fold) and 151 (−5.0-fold) when compared to control osteoblasts (Table 4). These miR findings are consistent with the inhibition of osteoblast differentiation, maturation, and function in $Pthrp^{\Delta/\Delta}$ osteoblasts (Table 4).

$Pthrp^{\Delta/\Delta}$ BMSCs produced a greater number of adipocytes, but displayed abnormal lipid metabolism

$Pthrp^{\Delta/\Delta}$ BMSCs produced a greater number of adipocytes that expressed more *Pparγ* and *aP2*, but less *Lpl* ($p \leq 0.042$) when compared to control BMSC-derived adipocytes (Figure 2). However, both genotypes expressed similar *C/ebpα*, *C/ebpβ*, *adipsin*, *Pthrp*, and *Pth1r*.

$Pthrp^{\Delta/\Delta}$ adipocytes expressed greater amounts of miR-221 (+34-fold), 132 (+3.5-fold), 434 (+2.7-fold), and 222 (+2.5-fold) when compared to control adipocytes. Adipocytes derived from $Pthrp^{\Delta/\Delta}$ BMSCs also expressed lower amounts of miR-210 (−2.5-fold), 30e (−2.5-fold), 19a (−2.5-fold), 17 (−3.3-fold), 20a (−3.3-fold), 101b (−3.3-fold), 106b (−3.3-fold), 27b (−5.0-fold), and 34c (−5.0-fold) when compared to those derived from control BMSCs (Table 4). This miR signature in $Pthrp^{\Delta/\Delta}$ adipocytes is consistent with increased adipogenesis, but also reflects abnormalities in lipid metabolism (Table 4).

Chondrocytes differentiated from $Pthrp^{\Delta/\Delta}$ BMSCs had decreased cartilage formation

Cartilage pellets grown from $Pthrp^{\Delta/\Delta}$ BMSCs were significantly smaller than those grown from control BMSCs ($p = 0.001$) (Figure 3). Histologic and IHC analyses demonstrated chondrogenesis based on the pellets consisting of a population of round cells with both intra- and extracellular alcian blue and type II collagen staining. While $Pthrp^{\Delta/\Delta}$ cartilage pellets had a smaller cross-sectional area and greater cell density, control pellets demonstrated a (1) lower cell density, (2) greater cross-sectional area, and (3) larger overall amount of extracellular matrix (ECM). $Pthrp^{\Delta/\Delta}$ BMSC-derived chondrocytes expressed less *Sox9* and *Pth1r* and a greater amount of *Col2a1* ($p \leq 0.024$); however, they expressed similar levels of *Pthrp* and *Agg* as control chondrocytes (Figure 3).

Sequencing of the miR population in $Pthrp^{\Delta/\Delta}$ chondrocytes demonstrated a marked increase in the anti-osteochondrogenic miR number 204 (+12-fold) and also an increase in 450a (+3.7-fold), 196a (+2.9-fold), 146b (+2.9-fold), 324 (+2.8-fold), 30e (+2.5-fold), and 140 (+2.5-fold) and decrease in miR-155, 221, let-7g, let-7f, and miR-15b (all −2.5-fold) when compared to control chondrocytes (Table 4). Differences in miRs in $Pthrp^{\Delta/\Delta}$ chondrocytes indicate the inhibition of differentiation, similar to the morphometric and gene expression analyses (Table 4).

$Pthrp^{\Delta/\Delta}$ BMSCs produced a greater number of myocytes, expressed higher levels of myogenic genes, and had an miR signature reflecting increased myogenesis

$Pthrp^{\Delta/\Delta}$ BMSCs displayed significantly less desmin positivity at baseline when compared to control BMSCs by flow cytometric analysis ($p = 0.001$) (Figure 4). However, myogenic induction was significantly stronger in $Pthrp^{\Delta/\Delta}$ BMSCs during myogenic differentiation for 24 days. This was evident in a significant increase in the fold change in desmin-positive cells over time in $Pthrp^{\Delta/\Delta}$ cultures when compared to controls (16.8 vs 2.3-fold, $p < 0.0001$). This

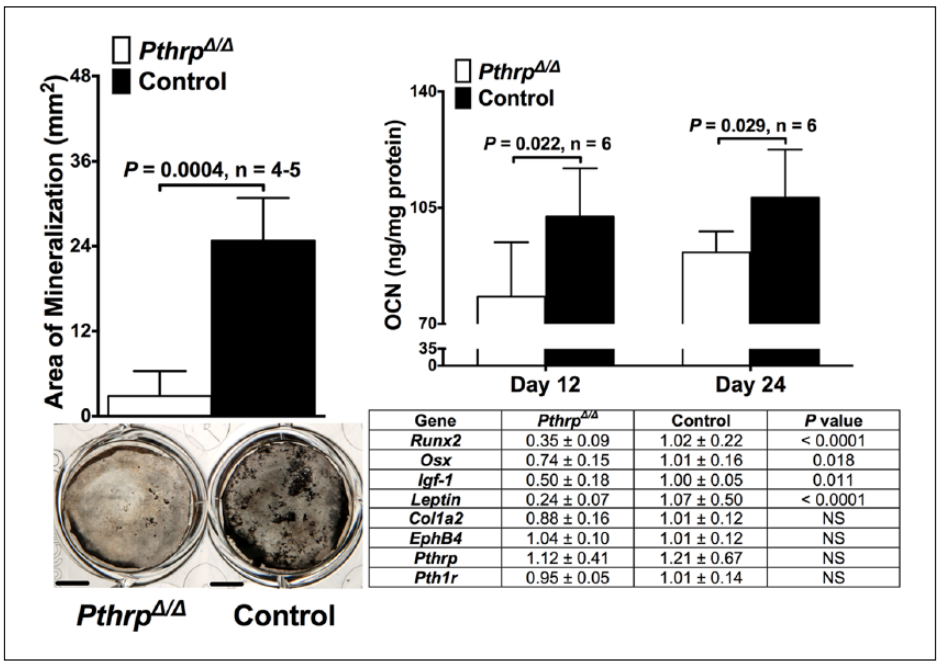

Gene	*Pthrp*$^{\Delta/\Delta}$	Control	*P* value
Runx2	0.35 ± 0.09	1.02 ± 0.22	< 0.0001
Osx	0.74 ± 0.15	1.01 ± 0.16	0.018
Igf-1	0.50 ± 0.18	1.00 ± 0.05	0.011
Leptin	0.24 ± 0.07	1.07 ± 0.50	< 0.0001
Col1a2	0.88 ± 0.16	1.01 ± 0.12	NS
EphB4	1.04 ± 0.10	1.01 ± 0.12	NS
Pthrp	1.12 ± 0.41	1.21 ± 0.67	NS
Pth1r	0.95 ± 0.05	1.01 ± 0.14	NS

Figure 1. Area of mineralization, representative images of von Kossa–stained wells, OCN secretion, and the expression of osteogenesis genes in both *Pthrp*$^{\Delta/\Delta}$ and control osteoblasts after BMSC differentiation. *Pthrp*$^{\Delta/\Delta}$ osteoblasts have decreased osteoblast differentiation, maturation, function, and bone formation. Bars represent mean ± SD of four to five replicates for area of mineralization and six replicates for OCN secretion. Measurement bars equal 5 mm. Within the table, values represent mean ± SD of five to six replicates for gene expression analysis. For all figures, findings are representative of two independent experiments.

Table 4. miR sequencing of differentiation assays.

miR sequencing of osteogenesis assays				
miR	*Pthrp*$^{\Delta/\Delta}$	Control	Fold	Predicted effect of difference based on function in osteogenesis
miR-204	5888	894	+6.6	Inhibition of osteoblast differentiation by inhibiting *Runx2*
miR-450a	5542	1384	+4.0	None specific for osteogenesis; compensatory to reduce proliferation
miR-410	1941	537	+3.6	None specific for osteogenesis; however, increases myogenesis
miR-16-2	3300	1105	+3.0	Foreshortening of the mandible, as observed in *Pthrp*$^{\Delta/\Delta}$ mice
miR-18a	1484	528	+2.8	Inhibition of osteoblast differentiation by inhibiting *Igf-1*
miR-146b	35,899	13,127	+2.7	Inhibition of osteoblast differentiation by inhibiting *Fgf-2*, reducing *Taz*
miR-31	23,795	9011	+2.6	Inhibition of osteoblast differentiation by targeting *Satb2*
miR-19a	1321	524	+2.5	Reduced osteoblast function
miR-223	9073	22,515	−2.5	Reduced osteoblast maturation
miR-151	682	3306	−5.0	None specific for osteogenesis; linked to cell spreading and adhesion
miR sequencing of adipogenesis assays				
miR	*Pthrp*$^{\Delta/\Delta}$	Control	Fold	Predicted effect of difference based on function in adipogenesis
miR-221	33,719	999	+34	Increased in obesity, associated with development of insulin resistance
miR-132	2508	721	+3.5	Observed in diabetic and leptin-deficient mice
miR-434	2271	841	+2.7	Increasing adipocyte differentiation by inhibiting Wnt/β-catenin signaling
miR-222	2463	994	+2.5	Upregulated during obesity, correlates with expression of *Pparγ*
miR-210	1014	2496	−2.5	Observed in diabetic and leptin-deficient mice
miR-30e	1359	3388	−2.5	Increased pre-adipocyte growth, also is downregulated during obesity
miR-19a	698	1890	−2.5	Abnormal lipid and fatty acid metabolism
miR-17	1061	3088	−3.3	Downregulated during obesity, upregulated during osteogenic differentiation
miR-20a	1669	5547	−3.3	Upregulated during osteogenic differentiation
miR-101b	2182	7348	−3.3	None specific for adipocytes; increased in myogenesis
miR-106b	1290	4637	−3.3	Increased adipocyte differentiation

(Continued)

Table 4. (Continued)

miR sequencing of adipogenesis assays				
miR	*Pthrp*$^{\Delta/\Delta}$	Control	Fold	Predicted effect of difference based on function in adipogenesis
miR-27b	761	3556	−5.0	Increased adipocyte differentiation by upregulation of *Pparγ*
miR-34c	864	4114	−5.0	Downregulated during adipogenesis
miR sequencing of chondrogenesis assays				
miR	*Pthrp*$^{\Delta/\Delta}$	Control	Fold	Predicted effect of difference based on function in chondrogenesis
miR-204	28,582	2331	+12	Inhibition of chondrocyte differentiation by inhibiting *Runx2*
miR-450a	4165	1126	+3.7	None specific for chondrogenesis; compensatory to reduce proliferation
miR-196a	2364	826	+2.9	None specific in mice; failure of appendage development in zebrafish
miR-146b	8162	2862	+2.9	Inhibition of chondrocyte differentiation by inhibiting *Fgf-2*
miR-324	1518	550	+2.8	None specific for chondrogenesis; increased during myogenesis
miR-30e	4284	1704	+2.5	None specific for chondrogenesis, inhibition of osteoblast differentiation
miR-140	1278	511	+2.5	Maintains chondrocytes in a proliferative state
miR-155	1020	2565	−2.5	None specific for chondrocytes, reduced osteoblast maturation
miR-221	12,347	31,815	−2.5	None specific for chondrocytes, reduced osteoblast function
let-7g	909	2393	−2.5	Decreased chondrogenesis, abnormal growth plate and skeletal development
let-7f	15,817	42,159	−2.5	Decreased chondrogenesis, abnormal growth plate and skeletal development
miR-15b	896	2420	−2.5	Inhibition of chondrocyte differentiation due to *Runx2* degradation
miR sequencing of myogenesis assays				
miR	*Pthrp*$^{\Delta/\Delta}$	Control	Fold	Predicted effect of difference based on function in myogenesis
miR-155	5751	1551	+3.7	Increased cardiomyogenesis, also inhibits adipogenesis
let-7e	2987	913	+3.3	Increased cardiomyocyte differentiation
miR-99b	4818	1544	+3.1	Increased cardiomyocyte differentiation
miR-30a	5348	13,428	−2.5	Downregulation induces cardiomyocyte hypertrophy
miR-214	1324	3333	−2.5	Prevents myocyte cell cycle exit, increasing proliferation and cell size
miR-34b	788	2029	−2.6	Increased cardiomyocyte survival
miR-193b	651	1717	−2.6	Increased myogenic differentiation
miR-328	786	2131	−2.7	Compensatory decrease to reduce cardiomyocyte hypertrophy
miR-34c	2550	10,225	−4.0	Increased cardiomyocyte survival

miR: microRNA.
The number of *Pthrp*$^{\Delta/\Delta}$ and control reads per million miR reads for each miR are reported. Fold differences were calculated by dividing the number of *Pthrp*$^{\Delta/\Delta}$ reads by the number of control reads for each miR. The predicted effect indicates what this fold difference for each miR should indicate in *Pthrp*$^{\Delta/\Delta}$ osteoblasts, adipocytes, chondrocytes, and myocytes.

ultimately resulted in a greater number of desmin-positive *Pthrp*$^{\Delta/\Delta}$ myocytes when compared to controls at day 24 when measured by flow cytometric analysis, a finding that was supported by anti-desmin cytochemistry ($p < 0.0001$) (Figure 4). *Pthrp*$^{\Delta/\Delta}$ myocytes expressed a greater amount of both *Des* and *Myog* ($p \leqslant 0.021$), but similar levels of *Pthrp* and *Pth1r* when compared to controls (Figure 4).

Pthrp$^{\Delta/\Delta}$ myocytes expressed greater amounts of miR-155 (+3.7-fold), let-7e (+3.3-fold), and 99b (+3.1-fold), but a lower amount of miR-30a (−2.5-fold), 214-3 (−2.5-fold), 34b (−2.6-fold), 193b (−2.6-fold), 328 (−2.7-fold), and 34c (−4.0-fold) than control myocytes (Table 4). The miR signature in *Pthrp*$^{\Delta/\Delta}$ myocytes indicates increased myocyte differentiation and survival (Table 4).

Discussion

BMSC differentiation requires the coordinated interaction of stage-specific regulatory and intrinsic genetic factors. However, the mechanisms controlling lineage specification are not fully understood. In this study, we demonstrated that BMSCs isolated from *Pthrp*$^{\Delta/\Delta}$ mice have an anti-osteogenic, anti-chondrogenic, pro-adipogenic, and pro-myogenic phenotype. This same phenotype is also observed when *Pthrp*$^{\Delta/\Delta}$ BMSCs were subjected to lineage-specific differentiation assays. These results indicate that the NLS and C-terminus of PTHrP are required for the proper multilineage differentiation of BMSCs.

Pthrp$^{\Delta/\Delta}$ and control BMSCs and their differentiated osteoblasts, adipocytes, chondrocytes, and myocytes express

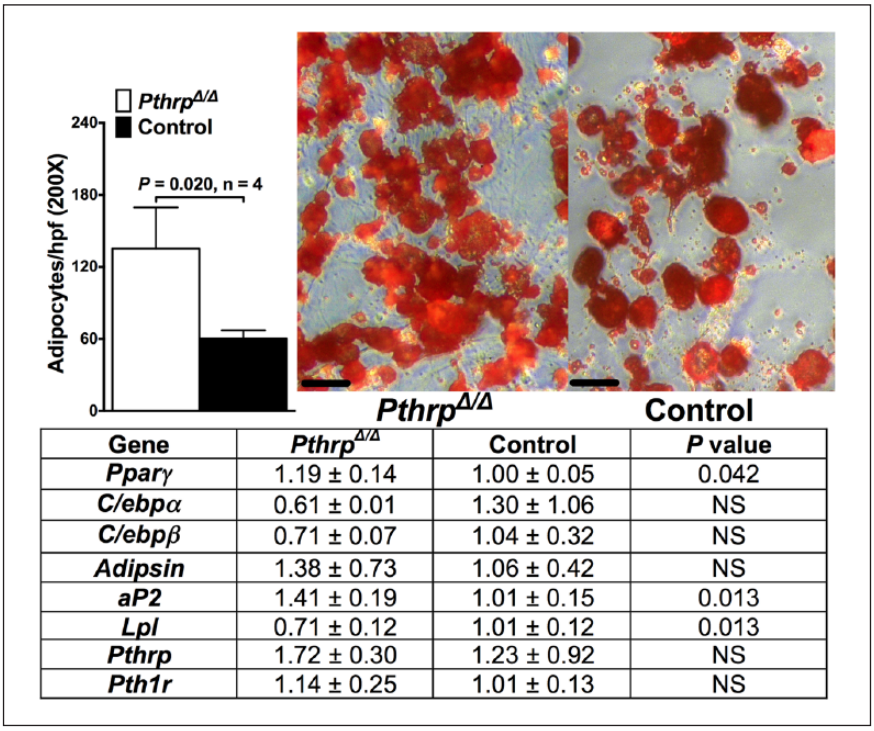

Gene	*Pthrp*$^{\Delta/\Delta}$	Control	*P* value
Pparγ	1.19 ± 0.14	1.00 ± 0.05	0.042
C/ebpα	0.61 ± 0.01	1.30 ± 1.06	NS
C/ebpβ	0.71 ± 0.07	1.04 ± 0.32	NS
Adipsin	1.38 ± 0.73	1.06 ± 0.42	NS
aP2	1.41 ± 0.19	1.01 ± 0.15	0.013
Lpl	0.71 ± 0.12	1.01 ± 0.12	0.013
Pthrp	1.72 ± 0.30	1.23 ± 0.92	NS
Pth1r	1.14 ± 0.25	1.01 ± 0.13	NS

Figure 2. Adipocyte number, representative images of Oil Red O–stained adipocytes, and the expression of adipogenesis genes in both *Pthrp*$^{\Delta/\Delta}$ and control adipocytes after BMSC differentiation. Despite a greater number of *Pthrp*$^{\Delta/\Delta}$ adipocytes and increased expression of *Pparγ* and *aP2, Pthrp*$^{\Delta/\Delta}$ adipocytes expressed less *Lpl* and similar levels of *C/ebpα*, *C/ebpβ*, and *adipsin*, suggesting dysregulated energy metabolism. Bars represent mean ± SD of four replicates for adipocyte number. Measurement bars represent 50 µm. Within the table, values represent mean ± SD of four replicates for gene expression analysis.

similar levels of *Pthrp*. This is in accordance with our previously published observations that *Pthrp*$^{\Delta/\Delta}$ and control mice have similar (1) plasma concentrations of PTHrP (<3 pM); (2) secretion of PTHrP from fibroblasts; (3) immunostaining for PTHrP in skin, fibroblasts, and respiratory epithelia; and (4) mRNA and protein levels of PTHrP in tibial metaphyses and calvaria.[4] We have also determined that the PTHrP concentration in the FBS used in all media in this study was <1 pM. This indicates that any differences between *Pthrp*$^{\Delta/\Delta}$ and controls in this study resulted from *Pthrp*$^{\Delta/\Delta}$ mice lacking the NLS and C-terminus of PTHrP and were not the result of (1) differences in PTHrP expression between genotypes or (2) exogenous PTHrP present within the FBS. PTH1R signaling activates two classic G-protein signaling cascades, the adenylate cyclase (AC) and phospholipase C (PLC) pathways. Stimulation of AC signaling leads to the activation of protein kinase A (PKA) and intracellular cyclic adenosine monophosphate (cAMP) accumulation. Increased PLC signaling leads to the activation of protein kinase C (PKC) and the increase in intracellular calcium. It has been previously demonstrated that PTHrP peptides of various length have indistinguishable biological effects on the activation of PTH1R, as long as there is an intact PTHrP 1-34 within the peptide. More specifically, the effects of N-terminal PTHrP 1-34, PTHrP 1-108, and full-length PTHrP 1-141 on AC and PLC signaling are equivalent, as noted in many studies by their equivalent biological effects in increasing (1) intracellular cAMP (AC/PKA pathway activation) and (2) intracellular calcium (PLC/PKC stimulation).[23–28] However, administration of PTHrP analogs containing only the NLS or C-terminus has no effect on intracellular cAMP or calcium, indicating no effects on PTH1R signaling by the NLS or C-terminus of PTHrP.[25,28] Considering this, the absence of a decrease in *Pka* and *Pkc* expression in *Pthrp*$^{\Delta/\Delta}$ BMSCs, and historical data on the effects of different lengths of PTHrP on PTH1R signaling, we believe that our findings in *Pthrp*$^{\Delta/\Delta}$ mice result from (1) the lack of the intracellular intracrine effects of the protein or (2) PTH1R-independent effects due to the absence of the NLS and C-terminus of PTHrP and are not due to differences in PTHrP expression, production, or decreased signaling through PTH1R.

Pthrp$^{\Delta/\Delta}$ BMSCs have significantly higher *Gsk-3β* but lower *β-catenin* expression. Based on the known function of these genes in the regulation of BMSC differentiation by canonical Wnt/β-catenin signaling, this expression pattern of *Gsk-3β* and *β-catenin* could contribute to the

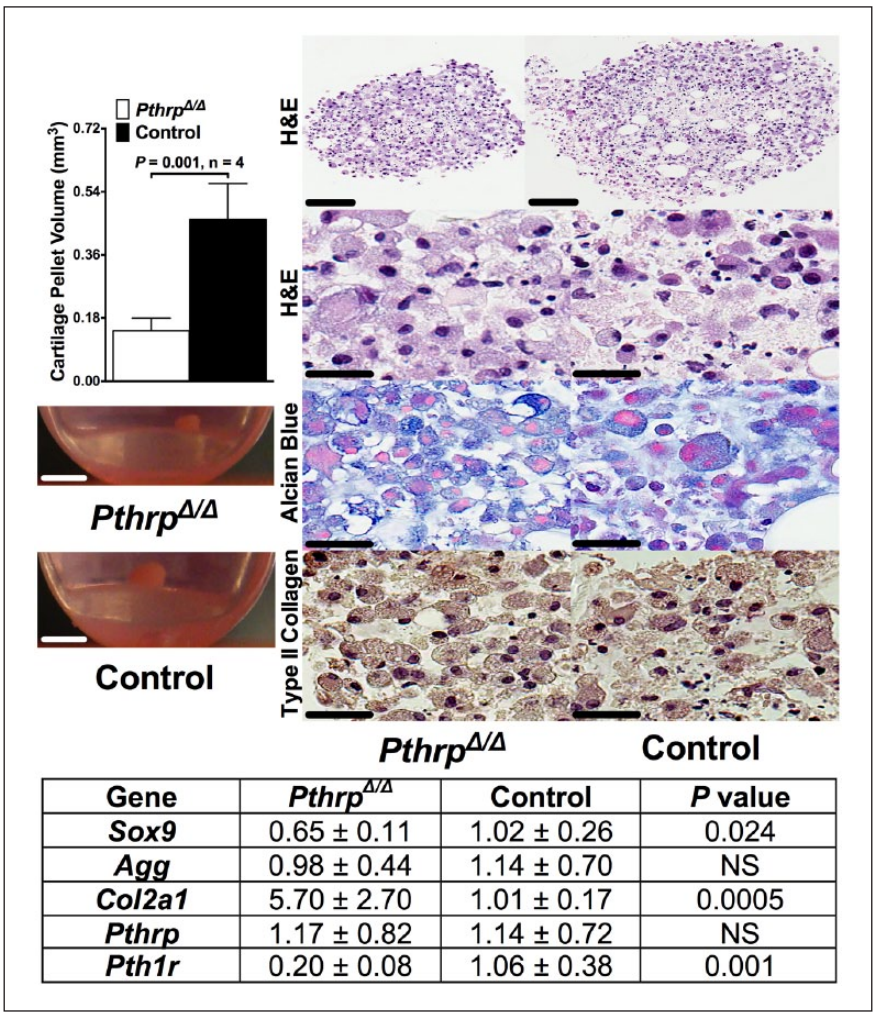

Gene	*Pthrp*$^{\Delta/\Delta}$	Control	*P* value
Sox9	0.65 ± 0.11	1.02 ± 0.26	0.024
Agg	0.98 ± 0.44	1.14 ± 0.70	NS
Col2a1	5.70 ± 2.70	1.01 ± 0.17	0.0005
Pthrp	1.17 ± 0.82	1.14 ± 0.72	NS
Pth1r	0.20 ± 0.08	1.06 ± 0.38	0.001

Figure 3. Cartilage pellet volume, representative pellet, H&E, alcian blue, and anti-type II collagen-stained section images, and the expression of chondrogenesis genes in both *Pthrp*$^{\Delta/\Delta}$ and control chondrocytes after BMSC differentiation. Despite a reduced (1) cartilage pellet volume, (2) cross-sectional area, and (3) amount of ECM in *Pthrp*$^{\Delta/\Delta}$ cartilage pellets in the face of greater cell density, *Pthrp*$^{\Delta/\Delta}$ chondrocytes expressed less *Sox9* and *Pth1r*, similar levels of *Pthrp* and *Agg*, and a greater amount of *Col2a1*. These cumulative findings are indicative of decreased chondrogenic differentiation and defective cartilage formation. For the alcian blue–stained sections, blue staining indicates the presence of glycosaminoglycans. For the type II collagen–stained sections, brown staining indicates type II collagen. Bars represent mean ± SD of four replicates for pellet volumes. Measurement bars indicate 1 mm for photographed cartilage pellet images, 100 µm for the top row of the H&E-stained histologic images, and 25 µm for all other H&E-, alcian blue-, and type II collagen-stained histologic sections. Values represent mean ± SD of three to four replicates for gene expression analysis in the table.

decreased osteochondrogenesis and increased adipogenesis observed in *Pthrp*$^{\Delta/\Delta}$ BMSCs. *Pthrp*$^{\Delta/\Delta}$ BMSCs expressed less *Taz* than control BMSCs. TAZ activates *Runx2* and inhibits *Pparγ*, increasing osteogenesis and decreasing adipogenesis.[29] Therefore, decreased *Taz* may contribute to the reduction in osteogenesis and increased adipogenesis observed in *Pthrp*$^{\Delta/\Delta}$ BMSCs.

The expression of the gp130 cytokines OSM, CT-1, and LIF was also altered in *Pthrp*$^{\Delta/\Delta}$ BMSCs. OSM is pro-osteogenic and anti-adipogenic through both its receptor and by indirectly increasing canonical Wnt/β-catenin signalling.[30,31] We found decreased *Osm* in *Pthrp*$^{\Delta/\Delta}$ BMSCs, supporting our phenotypic findings. CT-1 increases cardiomyocyte differentiation.[32] Therefore, increased *Ct-1* expression supports *Pthrp*$^{\Delta/\Delta}$ BMSCs' pro-myogenic phenotype. We also found increased *Lif* expression in *Pthrp*$^{\Delta/\Delta}$ BMSCs, consistent with its pro-adipogenic, pro-myogenic, and anti-osteogenic effects.[33,34] *Klf4* was also increased in *Pthrp*$^{\Delta/\Delta}$ BMSCs, which increases adipogenesis and myogenesis.[35,36]

We found increased *Pth1r* and *Lrp6* expression in *Pthrp*$^{\Delta/\Delta}$ BMSCs. Increased *Zfp521* in *Pthrp*$^{\Delta/\Delta}$ BMSCs likely results from increased *Pth1r* and supports the decreased osteogenesis and increased chondrocyte proliferation with less maturation. This is due to Zfp521 acting downstream of PTH1R to antagonize Runx2, thereby sustaining chondrocyte proliferation.[37] Increased *Pth1r* and *Lrp6* in *Pthrp*$^{\Delta/\Delta}$ BMSCs may result from decreased *Igf-1*,

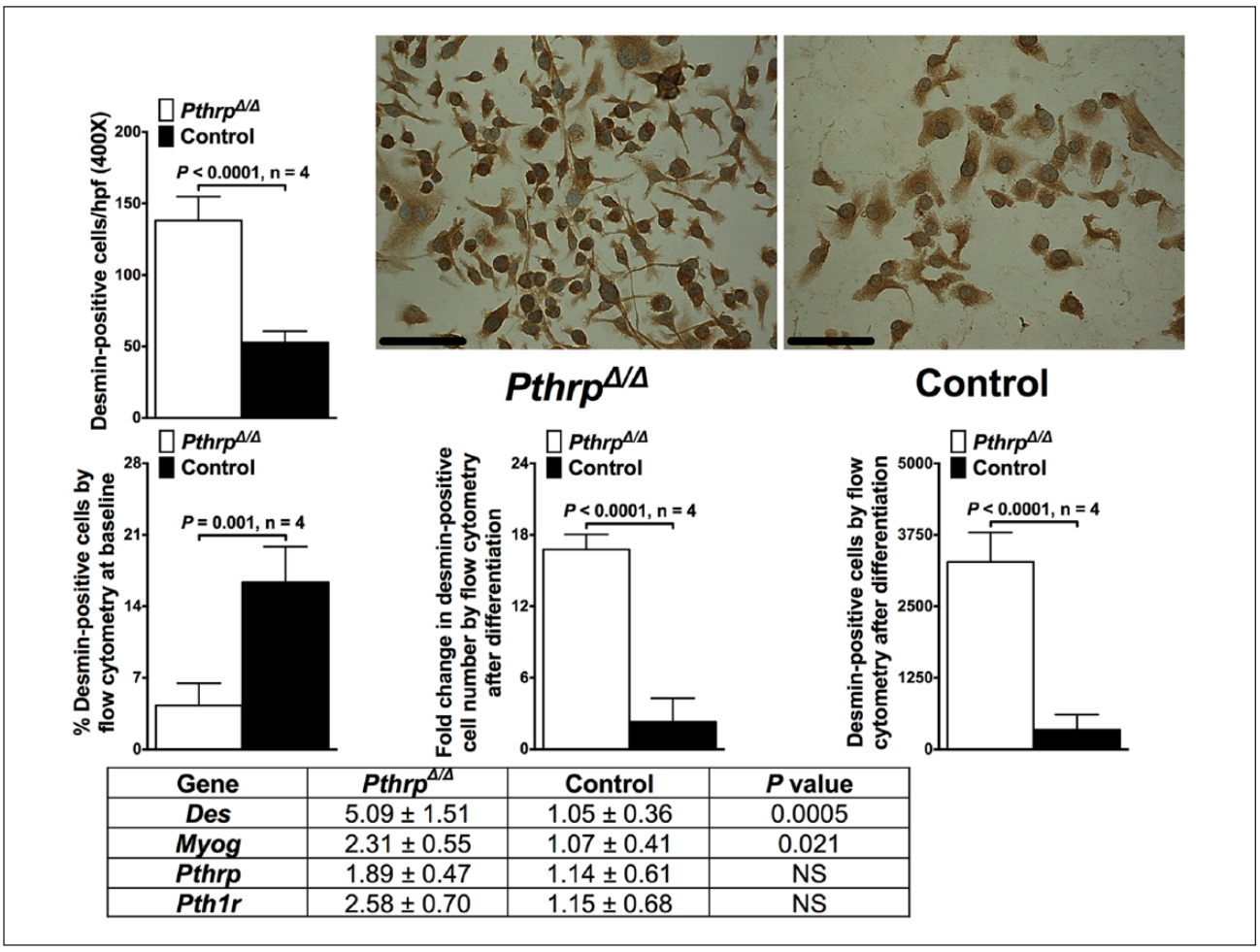

Gene	*Pthrp*$^{\Delta/\Delta}$	Control	*P* value
Des	5.09 ± 1.51	1.05 ± 0.36	0.0005
Myog	2.31 ± 0.55	1.07 ± 0.41	0.021
Pthrp	1.89 ± 0.47	1.14 ± 0.61	NS
Pth1r	2.58 ± 0.70	1.15 ± 0.68	NS

Figure 4. Myocyte quantification by both anti-desmin cytochemistry and flow cytometry, representative images of desmin-positive cells and the expression of myogenic genes in both *Pthrp*$^{\Delta/\Delta}$ and control myocytes after BMSC differentiation. Results showed increased myogenesis in the *Pthrp*$^{\Delta/\Delta}$ group by cytochemistry, flow cytometry (both by the increase in fold change in the number of desmin-positive cells over time and ultimately the number of desmin-positive cells after 24 days of myogenic differentiation), and the expression of *Des* and *Myog*. Bars represent mean ± SD of four replicates for both myocyte cytochemistry and flow cytometry. Measurement bars denote 100 µm. Within the table, values represent mean ± SD of four replicates for gene expression analysis.

an inhibitor of *Pth1r*.[38] Since IGF-1 is pro-osteochondrogenic and anti-adipogenic, decreased *Igf-1* in *Pthrp*$^{\Delta/\Delta}$ BMSCs may contribute to their abnormal differentiation phenotype.[39] Further work is needed based on these findings to determine whether the NLS and C-terminus of PTHrP may regulate PTH1R by influencing IGF-1.

MiR sequencing revealed an anti-osteogenic, anti-chondrogenic, pro-adipogenic, and pro-myogenic miR signature in *Pthrp*$^{\Delta/\Delta}$ BMSCs, supporting our other findings. *Pthrp*$^{\Delta/\Delta}$ BMSCs had significantly less miR-22 and greater miR-434 than control BMSCs. miR-22 overexpression increases osteogenesis and decreases adipogenesis in BMSCs.[21] Therefore, reduced miR-22 in *Pthrp*$^{\Delta/\Delta}$ BMSCs is consistent with decreased osteogenesis and increased adipogenesis. miR-434 negatively regulates Stat3 in neural stem cells.[22] Stat3 is (1) activated by leptin, OSM, CT-1, and LIF and (2) essential for osteoblast and chondrocyte differentiation and function. Therefore, increased miR-434 supports our findings. We also showed increased expression of miR-30d and 199b with decreased miR-193b and 221 in *Pthrp*$^{\Delta/\Delta}$ BMSCs, consistent with decreased osteochondrogenesis (miR-30d, 199b), increased adipogenesis (miR-30d, 199b, 221), and increased myogenesis (miR-193b).[13,15,40,41]

Osteoblasts derived from *Pthrp*$^{\Delta/\Delta}$ BMSCs had significantly less mineralization area, *Runx2*, *Osx*, *Igf-1*, and *leptin* expression, and OCN secretion. Whereas Runx2 and Osx are transcriptional regulators essential for osteoblast differentiation, terminal maturation, and bone formation, OCN is highly expressed in mature osteoblasts, reflecting the degree of bone formation. Leptin, and as discussed previously with IGF-1, both enhance osteoblast differentiation at the expense of adipogenesis and regulate mature osteoblast function.[39,42] These findings are consistent with the decreased differentiation, maturation, and function observed in *Pthrp*$^{\Delta/\Delta}$ osteoblasts. These findings of decreased osteogenesis at the cytochemical and mRNA

level in *Pthrp*$^{\Delta/\Delta}$ BMSCs, which express PTHrP 1-66, are in accordance with a recent study that demonstrated decreased osteogenic differentiation in BMSCs isolated from mice with as not as severe truncation of the NLS and C-terminus of PTHrP (expresses PTHrP 1-84).[43]

Myogenesis involves the induction of genes critical for differentiation, including myogenin, and muscle-specific genes, including desmin. *Pthrp*$^{\Delta/\Delta}$ BMSCs also had increased expression of the pro-myogenic factors *Klf4*, *Ct-1*, and *Lif* and decreased canonical Wnt/β-catenin signaling, which increases myocyte differentiation.[32,34,36,44] This pro-myogenic gene signature ultimately led to a greater number of *Pthrp*$^{\Delta/\Delta}$ myocytes with increased *Des* and *Myog*. The pro-myogenic phenotype of *Pthrp*$^{\Delta/\Delta}$ BMSCs is further supported by our flow cytometric data. This revealed that despite a significant decrease in the percentage of desmin-positive cells at baseline in *Pthrp*$^{\Delta/\Delta}$ BMSCs when compared to control BMSCs, after 24 days of myogenic differentiation there was a robust increase in the number of desmin-positive cells in *Pthrp*$^{\Delta/\Delta}$ cultures grown in parallel with control BMSCs (16.8 vs 2.3-fold, respectively). This resulted in a greater number of *Pthrp*$^{\Delta/\Delta}$ myocytes than control myocytes after 24 days of differentiation, which was supported by anti-desmin cytochemical staining.

Chondrocytes derived from *Pthrp*$^{\Delta/\Delta}$ BMSCs had less differentiation and formation, as observed in decreased *Sox9* expression and cartilage pellet volume. Histologically, *Pthrp*$^{\Delta/\Delta}$ cartilage pellets had a (1) greater cell number per area and (2) lesser amount of ECM per area when compared to control pellets. These findings demonstrate decreased ECM production by *Pthrp*$^{\Delta/\Delta}$ chondrocytes. Despite both genotypes having similar levels of *Agg* expression, *Pthrp*$^{\Delta/\Delta}$ chondrocytes expressed greater *Col2a1*. This increase in *Col2a1* in *Pthrp*$^{\Delta/\Delta}$ chondrocytes with a concurrent decrease in ECM production within *Pthrp*$^{\Delta/\Delta}$ pellets indicates defective chondrogenesis. *Pthrp*$^{\Delta/\Delta}$ chondrocytes also had decreased *Pth1r* expression. This finding is in contrast to *Pthrp*$^{\Delta/\Delta}$ and control osteoblasts, adipocytes, and myocytes, which express similar levels of *Pth1r*. However, this reduction in *Pth1r* in *Pthrp*$^{\Delta/\Delta}$ chondrocytes was similar to that observed in the largely cartilaginous embryonic skeletons of mice expressing a similar truncation of PTHrP, PTHrP 1-84, which also possess a chondrodysplastic phenotype.[45] These similarities of decreased *Pth1r* but similar *Pthrp* in cartilaginous tissues from both mouse models suggest that the absence of the NLS and C-terminus of PTHrP and decreased *Pth1r* in chondrocytes may both contribute to the decreased chondrogenesis in mice lacking the NLS and C-terminus of PTHrP. In summary, these cumulative findings are indicative of decreased chondrogenic differentiation in and defective cartilage formation by *Pthrp*$^{\Delta/\Delta}$ BMSC-derived chondrocytes.

Measurement of miRs following differentiation revealed changes that paralleled the in vitro and in vivo phenotype of *Pthrp*$^{\Delta/\Delta}$ cells and mice. Osteogenesis assays of *Pthrp*$^{\Delta/\Delta}$ BMSCs yielded an miR signature predicting inhibited osteoblast differentiation, maturation, and function. Known targets of miR-204 and 18a, which were both upregulated in *Pthrp*$^{\Delta/\Delta}$ osteoblasts, include *Runx2* and *Igf-1*, respectively, which were both downregulated at the mRNA level in *Pthrp*$^{\Delta/\Delta}$ osteoblasts.[9,46,47] Osx negatively regulates miR-204.[9] Increased miR-204 with decreased *Osx* in *Pthrp*$^{\Delta/\Delta}$ osteoblasts suggests that the NLS and C-terminus may regulate miR-204 through *Osx*. Therefore, the NLS and C-terminus of PTHrP regulate miRs important for osteoblast commitment, differentiation, and function. *Pthrp*$^{\Delta/\Delta}$ adipocytes had an miR signature consistent with our findings of increased adipocyte differentiation due to upregulation of *Pparγ* (decreased miR-27b) and increased adipogenesis (decreased miR-34c).[10,11] *Pthrp*$^{\Delta/\Delta}$ adipocyte miR changes, most notably the increase in miR-221 and 132, were consistent with obesity, diabetes, and decreases in leptin.[48,49] Similar to gene, morphometric, and histologic changes in *Pthrp*$^{\Delta/\Delta}$ chondrogenesis assays, miR changes predicted inhibited differentiation and increased proliferation.[9,14] Several identified miRs in *Pthrp*$^{\Delta/\Delta}$ chondrocytes are linked to decreased osteoblast differentiation, maturation, and function. This is not surprising since many factors regulating chondrocyte differentiation also regulate osteoblast differentiation. The marked increase in miR-204 in *Pthrp*$^{\Delta/\Delta}$ chondrocytes was consistent with findings in *Pthrp*$^{\Delta/\Delta}$ osteoblasts and with miR-204 decreasing osteochondrogenesis.[9] Decreases in let-7 miRs are linked to reduced and abnormal growth plate chondrogenesis.[12] Further work is needed to determine whether the abnormal growth plate chondrogenesis and skeletal morphogenesis in *Pthrp*$^{\Delta/\Delta}$ mice are due to a decrease in let-7 miRs resulting from the absence of the NLS and C-terminus of PTHrP. The changes in miRs in *Pthrp*$^{\Delta/\Delta}$ myocytes predict increased myocyte differentiation and survival, consistent with our other findings.[50,51]

In addition to BMSC differentiation, a bone–fat connection exists.[52] Osteoblast-derived OCN stimulates insulin and adipokine production, fat reduction, and skeletal muscle to uptake glucose.[52] Adipocytes secrete adipokines such as leptin and adipsin. *Pparγ* transcriptionally controls adipogenesis, governing regulators of energy and lipid metabolism and insulin sensitivity such as *Lpl* and *aP2*.[53] Increased *Pparγ*, with no increase in *adipsin* and a decrease in *Lpl* in *Pthrp*$^{\Delta/\Delta}$ adipocytes, suggests that the NLS and C-terminus of PTHrP are required for proper adipocyte function and regulate genes involved in metabolism. Consistent with our findings, an increase in *Pparγ* in the long bones of mice expressing only PTHrP 1-84, when compared to PTHrP 1-66, was recently reported.[43] Therefore, adipogenesis gene expression similarities, adipogenesis miR changes, and decreased *leptin* expression and OCN secretion in *Pthrp*$^{\Delta/\Delta}$ osteoblasts, despite a greater number of *Pthrp*$^{\Delta/\Delta}$ adipocytes, suggest dysregulated energy

metabolism. This may contribute to the perinatal lethality in *Pthrp*$^{\Delta/\Delta}$ mice.[4]

In conclusion, the presence of an intact NLS and C-terminus of PTHrP is required for normal BMSC differentiation. Multiple genes, miRs, and signaling pathways central to the normal function of BMSCs and their progeny are altered following the deletion of the NLS and C-terminus of PTHrP. The creation of mice lacking each specific region of PTHrP, alone or in combination, and their comparison to the original PTHrP knockout mice, PTH1R knockout mice, and our *Pthrp*$^{\Delta/\Delta}$ mice and age-matched controls would help to elucidate which region or regions of PTHrP have the greatest involvement in regulating BMSC differentiation. This is the first study to identify changes in miR expression following the modification of PTHrP, and more specifically, deletion of the NLS and C-terminus. Identification of factors regulating BMSC differentiation is of paramount importance for the development of treatment strategies for a variety of musculoskeletal and metabolic conditions. Targeting, overexpressing, or administration of the NLS and C-terminus of PTHrP in peptide form may be promising strategies to generate specific tissue types in the field of regenerative medicine.

Acknowledgements

The authors would like to thank Michael J. Fial for technical assistance with flow cytometry and Selen Yilmaz for technical assistance with microRNA sequencing. The conception and design of the work reported in this article was by B.E.H., T.J.R., and R.E.T. All authors were involved in data acquisition, analysis, and interpretation. B.E.H. wrote the article and it was then revised critically by all the authors. All authors approved the final version of the article to be published.

Declaration of conflicting interests

The author(s) declared no potential conflicts of interest with respect to the research, authorship, and/or publication of this article.

Funding

The author(s) disclosed receipt of the following financial support for the research, authorship, and/or publication of this article: This work was funded by the National Institutes of Health to Drs B.E.H. (F32 AR057597) and R.E.T. (K01 RR018924). B.E.H. was also supported by the Ohio State University College of Veterinary Medicine C. Glenn Barber Fund. The authors would like to thank Alan Flechtner in our Comparative Pathology and Mouse Phenotyping Core Facility (supported by NIH CCC Grant P30 CA016058) for histologic processing.

References

1. Karaplis AC, Luz A, Glowacki J, et al. Lethal skeletal dysplasia from targeted disruption of the parathyroid hormone-related peptide gene. *Genes Dev* 1994; 8: 277–289.
2. Miao D, He B, Jiang Y, et al. Osteoblast-derived PTHrP is a potent endogenous bone anabolic agent that modifies the therapeutic efficacy of administered PTH 1-34. *J Clin Invest* 2005; 115: 2402–2411.
3. Wysolmerski JJ and Stewart AF. The physiology of parathyroid hormone-related protein: an emerging role as a developmental factor. *Annu Rev Physiol* 1998; 60: 431–460.
4. Toribio RE, Brown HA, Novince CM, et al. The midregion, nuclear localization sequence, and C terminus of PTHrP regulate skeletal development, hematopoiesis, and survival in mice. *FASEB J* 2010; 24: 1947–1957.
5. Schipani E, Lanske B, Hunzelman J, et al. Targeted expression of constitutively active receptors for parathyroid hormone and parathyroid hormone-related peptide delays endochondral bone formation and rescues mice that lack parathyroid hormone-related peptide. *Proc Natl Acad Sci U S A* 1997; 94: 13689–13694.
6. Amizuka N, Karaplis AC, Henderson JE, et al. Haploinsufficiency of parathyroid hormone-related peptide (PTHrP) results in abnormal postnatal bone development. *Dev Biol* 1996; 175: 166–176.
7. Chan GK, Miao D, Deckelbaum R, et al. Parathyroid hormone-related peptide interacts with bone morphogenetic protein 2 to increase osteoblastogenesis and decrease adipogenesis in pluripotent C3H10T 1/2 mesenchymal cells. *Endocrinology* 2003; 144: 5511–5520.
8. Kim YJ, Kim HJ and Im GI. PTHrP promotes chondrogenesis and suppresses hypertrophy from both bone marrow-derived and adipose tissue-derived MSCs. *Biochem Biophys Res Commun* 2008; 373: 104–108.
9. Chen Q, Liu W, Sinha KM, et al. Identification and characterization of microRNAs controlled by the osteoblast-specific transcription factor Osterix. *PLoS ONE* 2013; 8: e58104.
10. Karbiener M, Fischer C, Nowitsch S, et al. microRNA miR-27b impairs human adipocyte differentiation and targets PPARgamma. *Biochem Biophys Res Commun* 2009; 390: 247–251.
11. Keller P, Gburcik V, Petrovic N, et al. Gene-chip studies of adipogenesis-regulated microRNAs in mouse primary adipocytes and human obesity. *BMC Endocr Disord* 2011; 11: 7.
12. Papaioannou G, Inloes JB, Nakamura Y, et al. Let-7 and miR-140 microRNAs coordinately regulate skeletal development. *Proc Natl Acad Sci U S A* 2013; 110: E3291–E3300.
13. Sun L, Xie H, Mori MA, et al. Mir193b-365 is essential for brown fat differentiation. *Nat Cell Biol* 2011; 13: 958–965.
14. Yang J, Qin S, Yi C, et al. MiR-140 is co-expressed with Wwp2-C transcript and activated by Sox9 to target Sp1 in maintaining the chondrocyte proliferation. *FEBS Lett* 2011; 585: 2992–2997.
15. Zaragosi LE, Wdziekonski B, Brigand KL, et al. Small RNA sequencing reveals miR-642a-3p as a novel adipocyte-specific microRNA and miR-30 as a key regulator of human adipogenesis. *Genome Biol* 2011; 12: R64.
16. Hildreth BE III, Werbeck JL, Thudi NK, et al. PTHrP 1-141 and 1-86 increase in vitro bone formation. *J Surg Res* 2010; 162: e9–e17.
17. Peister A, Mellad JA, Larson BL, et al. Adult stem cells from bone marrow (MSCs) isolated from different strains of inbred mice vary in surface epitopes, rates of proliferation, and differentiation potential. *Blood* 2004; 103: 1662–1668.
18. Maggini J, Mirkin G, Bognanni I, et al. Mouse bone marrow-derived mesenchymal stromal cells turn activated

macrophages into a regulatory-like profile. *PLoS ONE* 2010; 5: e9252.
19. Roccaro AM, Sacco A, Maiso P, et al. BM mesenchymal stromal cell-derived exosomes facilitate multiple myeloma progression. *J Clin Invest* 2013; 123: 1542–1555.
20. Tondreau T, Lagneaux L, Dejeneffe M, et al. Isolation of BM mesenchymal stem cells by plastic adhesion or negative selection: phenotype, proliferation kinetics and differentiation potential. *Cytotherapy* 2004; 6: 372–379.
21. Huang S, Wang S, Bian C, et al. Upregulation of miR-22 promotes osteogenic differentiation and inhibits adipogenic differentiation of human adipose tissue-derived mesenchymal stem cells by repressing HDAC6 protein expression. *Stem Cells Dev* 2012; 21: 2531–2540.
22. Jovicic A, Roshan R, Moisoi N, et al. Comprehensive expression analyses of neural cell-type-specific miRNAs identify new determinants of the specification and maintenance of neuronal phenotypes. *J Neurosci* 2013; 33: 5127–5137.
23. Civitelli R, Martin TJ, Fausto A, et al. Parathyroid hormone-related peptide transiently increases cytosolic calcium in osteoblast-like cells: comparison with parathyroid hormone. *Endocrinology* 1989; 125: 1204–1210.
24. Ferrari S, Rizzoli R, Chaponnier C, et al. Parathyroid hormone-related protein increases cAMP production in mammary epithelial cells. *Am J Physiol* 1993; 264: E471–E475.
25. Maeda S, Wu S, Green J, et al. The N-terminal portion of parathyroid hormone-related protein mediates the inhibition of apical Na+/H+ exchange in opossum kidney cells. *J Am Soc Nephrol* 1998; 9: 175–181.
26. Rizzoli R, Ferrari SL, Pizurki L, et al. Actions of parathyroid hormone and parathyroid hormone-related protein. *J Endocrinol Invest* 1992; 15: 51–56.
27. Tsukazaki T, Ohtsuru A, Namba H, et al. Parathyroid hormone-related protein (PTHrP) action in rat articular chondrocytes: comparison of PTH(1-34), PTHrP(1-34), PTHrP(1-141), PTHrP(100-114) and antisense oligonucleotides against PTHrP. *J Endocrinol* 1996; 150: 359–368.
28. Wu S, Pirola CJ, Green J, et al. Effects of N-terminal, midregion, and C-terminal parathyroid hormone-related peptides on adenosine 3′,5′-monophosphate and cytoplasmic free calcium in rat aortic smooth muscle cells and UMR-106 osteoblast-like cells. *Endocrinology* 1993; 133: 2437–2444.
29. Hong JH and Yaffe MB. TAZ: a beta-catenin-like molecule that regulates mesenchymal stem cell differentiation. *Cell Cycle* 2006; 5: 176–179.
30. Song HY, Jeon ES, Kim JI, et al. Oncostatin M promotes osteogenesis and suppresses adipogenic differentiation of human adipose tissue-derived mesenchymal stem cells. *J Cell Biochem* 2007; 101: 1238–1251.
31. Walker EC, McGregor NE, Poulton IJ, et al. Oncostatin M promotes bone formation independently of resorption when signaling through leukemia inhibitory factor receptor in mice. *J Clin Invest* 2010; 120: 582–592.
32. Xinyun C, Zhi Z, Bin Z, et al. Effects of cardiotrophin-1 on differentiation and maturation of rat bone marrow mesenchymal stem cells induced with 5-azacytidine in vitro. *Int J Cardiol* 2010; 143: 171–177.
33. Falconi D, Oizumi K and Aubin JE. Leukemia inhibitory factor influences the fate choice of mesenchymal progenitor cells. *Stem Cells* 2007; 25: 305–312.
34. Spangenburg EE and Booth FW. Multiple signaling pathways mediate LIF-induced skeletal muscle satellite cell proliferation. *Am J Physiol Cell Physiol* 2002; 283: C204–C211.
35. Birsoy K, Chen Z and Friedman J. Transcriptional regulation of adipogenesis by KLF4. *Cell Metab* 2008; 7: 339–347.
36. Sunadome K, Yamamoto T, Ebisuya M, et al. ERK5 regulates muscle cell fusion through Klf transcription factors. *Dev Cell* 2011; 20: 192–205.
37. Seriwatanachai D, Densmore MJ, Sato T, et al. Deletion of Zfp521 rescues the growth plate phenotype in a mouse model of Jansen metaphyseal chondrodysplasia. *FASEB J* 2011; 25: 3057–3067.
38. Kawane T, Mimura J, Fujii-Kuriyama Y, et al. Identification of the promoter region of the parathyroid hormone receptor gene responsible for transcriptional suppression by insulin-like growth factor-I. *Arch Biochem Biophys* 2005; 439: 61–69.
39. Rosen CJ, Ackert-Bicknell CL, Adamo ML, et al. Congenic mice with low serum IGF-I have increased body fat, reduced bone mineral density, and an altered osteoblast differentiation program. *Bone* 2004; 35: 1046–1058.
40. Chou WW, Wang YT, Liao YC, et al. Decreased microRNA-221 is associated with high levels of TNF-alpha in human adipose tissue-derived mesenchymal stem cells from obese woman. *Cell Physiol Biochem* 2013; 32: 127–137.
41. Garzia L, Andolfo I, Cusanelli E, et al. MicroRNA-199b-5p impairs cancer stem cells through negative regulation of HES1 in medulloblastoma. *PLoS ONE* 2009; 4: e4998.
42. Thomas T, Gori F, Khosla S, et al. Leptin acts on human marrow stromal cells to enhance differentiation to osteoblasts and to inhibit differentiation to adipocytes. *Endocrinology* 1999; 140: 1630–1638.
43. Zhu M, Zhang J, Dong Z, et al. The p27 pathway modulates the regulation of skeletal growth and osteoblastic bone formation by parathyroid hormone-related peptide. *J Bone Miner Res*. Epub ahead of print 27 April 2015. DOI: 10.1002/jbmr.2544.
44. Cho J, Rameshwar P and Sadoshima J. Distinct roles of glycogen synthase kinase (GSK)-3alpha and GSK-3beta in mediating cardiomyocyte differentiation in murine bone marrow-derived mesenchymal stem cells. *J Biol Chem* 2009; 284: 36647–36658.
45. Miao D, Su H, He B, et al. Severe growth retardation and early lethality in mice lacking the nuclear localization sequence and C-terminus of PTH-related protein. *Proc Natl Acad Sci U S A* 2008; 105: 20309–20314.
46. Hu W, Li T, Wu L, et al. Identification of microRNA-18a as a novel regulator of the insulin-like growth factor-1 in the proliferation and regeneration of deer antler. *Biotechnol Lett* 2014; 36: 703–710.
47. Lei SF, Papasian CJ and Deng HW. Polymorphisms in predicted miRNA binding sites and osteoporosis. *J Bone Miner Res* 2011; 26: 72–78.
48. Meerson A, Traurig M, Ossowski V, et al. Human adipose microRNA-221 is upregulated in obesity and affects

fat metabolism downstream of leptin and TNF-alpha. *Diabetologia* 2013; 56: 1971–1979.
49. Nesca V, Guay C, Jacovetti C, et al. Identification of particular groups of microRNAs that positively or negatively impact on beta cell function in obese models of type 2 diabetes. *Diabetologia* 2013; 56: 2203–2212.
50. Drummond MJ, McCarthy JJ, Sinha M, et al. Aging and microRNA expression in human skeletal muscle: a microarray and bioinformatics analysis. *Physiol Genomics* 2011; 43: 595–603.
51. Iekushi K, Seeger F, Assmus B, et al. Regulation of cardiac microRNAs by bone marrow mononuclear cell therapy in myocardial infarction. *Circulation* 2012; 125: 1765–1773, S1–S7.
52. Lee NK and Karsenty G. Reciprocal regulation of bone and energy metabolism. *Trends Endocrinol Metab* 2008; 19: 161–166.
53. Rosen ED and MacDougald OA. Adipocyte differentiation from the inside out. *Nat Rev Mol Cell Biol* 2006; 7: 885–896.